Applied Mathematics and Computation 215 (2010) 4406–4421

Contents lists available at ScienceDirect

Applied Mathematics and Computation

journal homepage: www.elsevier.com/locate/amc

Elasto-plastic analysis of reinforced soils using mesh-free method

S.M. Binesh, N. Hataf *, A. Ghahramani

Civil Engineering Department, Shiraz University, Iran

ARTICLE INFO

Keywords:
Reinforced soil
Meshless method
Radial basis
Point interpolation
Elasto-plastic

ABSTRACT

In this paper the application of the mesh-free method (MFM) for the elasto-plastic analysis of reinforced soils is studied for the first time. The applied mesh-free method is called the radial point interpolation method (RPIM). In MFM, unlike the finite element method (FEM), there is no need of mesh in the traditional sense, and the shape functions are based on nodes. In the present study the reinforced soil is divided into three separate parts of soil, reinforcements, and interface layers. The displacement field in each part is constructed by RPIM. The final system of equations is derived by the substitution of the displacement field into the weak form of the governing equation. The elasto-plastic behaviors of soil, reinforcements, and interface layers are considered. There is also the ability of slippage modeling between the soil and reinforcement. Based on the derived equations a computer code has been developed and its validity investigated by solving some examples at the end of the paper.

1. Introduction

The use of fabric or polymer grid reinforcing material to improve the strength and stability of geotechnical structures is increasing. Generally, the investigation of the behavior of reinforced soil structures through field observation or laboratory modeling is expensive and time consuming. So it is necessary to develop numerical solutions which may be used to predict the load–deformation characteristics of reinforced soil structures. The most popular method for the numerical analysis of reinforced soils is the finite element method. Although FEM is widely used, there are some deficiencies such as the discontinuity of stresses on element boundaries, low accuracy at large deformation analysis or the weakness of the method in the two dimensional modeling of thin media (i.e. reinforcement). The mentioned shortcomings are mainly related to mesh definition. Therefore the authors have been encouraged to apply a new family of numerical methods, independent of mesh, for the analysis of reinforced soils. These new families of numerical methods are globally coined as mesh-free or meshless methods.

MFM were developed by Lucy [1] who introduced smoothed particle hydrodynamics (SPH) for modeling astrophysical phenomena. Libersky and Petschek [2] extended this method to solve the solid mechanics problem. Nayroles et al. [3] extended a new branch of MFM by using a basis function and a weight function to form a local approximation based on a set of nodes. Belytschko et al. [4] improved this method by introducing the moving least square approximation and called their method "element free Galerkin". Many other researchers proposed various MFMs such as finite cloud [5], reproducing kernel particle method [6], the point interpolation method [7], etc. Their main characteristic is that there is no need of mesh in the traditional sense.

There has been a great deal of research into the application of MFMs in different fields of science. Among these, a few are devoted to the application of MFMs in geotechnical engineering. Zhang et al. [8] analyzed a two dimensional model of jointed

* Corresponding author.
E-mail addresses: nhataf@gmail.com, nhataf@shirazu.ac.ir (N. Hataf).

0096-3003/$ - see front matter © 2010 Elsevier Inc. All rights reserved.
doi:10.1016/j.amc.2010.01.004

rock mass by the element-free Galerkin method. Hataf et al. [9] extended Zhang's method to the elasto-plastic behavior of joints. Wang et al. [10,11], in different studies, used the point interpolation method for consolidation process modeling. Guangxin et al. [12] applied the mesh-free method to the free surface seepage analysis. Wiezckowski [13] used the material point method for the analysis of large strain problems such as pile driving in soil mechanics. Binesh et al. [14,15] performed an elastic analysis of the reinforced soils and the discontinuous mediums using the point interpolation method.

In this paper the authors extended the previous work [14] to the elasto-plastic analysis of reinforced soil structures and also to the slippage modeling of the interface. The radial point interpolation method (RPIM), which is enriched by polynomial terms, is used for the construction of shape functions. The system of equations has been derived and a code has been developed based on RPIM. The validity of the developed code has been investigated by solving some examples at the end of the paper.

2. Point interpolation method (PIM)

Polynomials have been used as basis functions in interpolation to create shape functions in many numerical methods such as FEM. In the FEM, however, the interpolation is based on elements that have no gap and overlapping. In PIM, interpolation is based on a small set of nodes in the vicinity of a desired point named local support domain (Fig. 1). Support domains of different points can overlap each other.

Consider a continuous function $u(\mathbf{X})$ (i.e. displacement function). This function can be approximated in the vicinity of $\mathbf{X}$ as follows:

$$u(\mathbf{X}) = \sum_{i=1}^{n} p_i(\mathbf{X}) a_i = \mathbf{P}^T \mathbf{a}, \tag{1}$$

where $p_i(\mathbf{X})$ is the polynomial basis function of $\mathbf{X} = [x, y]^T$, n is the number of nodes in the support domain of X, and a_i is the corresponding coefficient of the basis function. The unknown coefficient a_i in Eq. (1), can be determined by enforcing $u(\mathbf{X})$ to be the nodal displacement at n nodes in the support domain. It can then be written as

$$\mathbf{U}_S = \mathbf{P}_Q \mathbf{a}, \tag{2}$$

where $\mathbf{U}_S$ is the vector of nodal displacements,

$$\mathbf{U}_S = \{u_1 \quad u_2 \quad u_3 \quad \dots \quad u_n\}^T, \tag{3}$$

$\mathbf{a}$ is the vector of unknown coefficients,

$$\mathbf{a} = \{a_1 \quad a_2 \quad a_3 \quad \dots \quad a_n\}^T \tag{4}$$

and $\mathbf{P}_Q$ is the polynomial moment matrix

$$\mathbf{P}_Q = \begin{bmatrix} 1 & x_1 & y_1 & x_1 y_1 & \cdots & p_n(\mathbf{X}_1) \\ 1 & x_2 & y_2 & x_2 y_2 & \cdots & p_n(\mathbf{X}_2) \\ 1 & x_3 & y_3 & x_3 y_3 & \cdots & p_n(\mathbf{X}_3) \\ \vdots & \vdots & \vdots & \vdots & & \vdots \\ 1 & x_n & y_n & x_n y_n & \cdots & p_n(\mathbf{X}_n) \end{bmatrix}. \tag{5}$$

Assuming the existence of P_Q^{-1}, a unique solution of $\mathbf{a}$ can be obtained as

$$\mathbf{a} = \mathbf{P}_Q^{-1} \mathbf{U}_S. \tag{6}$$

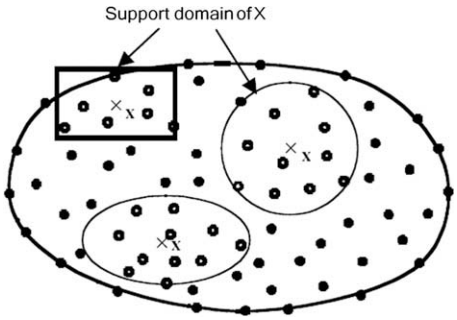

Fig. 1. Support domain of point X.

Substituting Eq. (6) into Eq. (1) yields

$$u(\mathbf{X}) = \mathbf{P}^T(\mathbf{X})\mathbf{P}_Q^{-1}\mathbf{U}_S = \sum_{i=1}^{n} \varphi_i u_i = \mathbf{\Phi}^T(\mathbf{X})\mathbf{U}_S, \tag{7}$$

where $\mathbf{\Phi}(\mathbf{X})$ is the vector of PIM shape functions

$$\mathbf{\Phi}^T(\mathbf{X}) = \{\varphi_1(\mathbf{X}) \quad \varphi_2(\mathbf{X}) \quad \dots \quad \varphi_n(\mathbf{X})\}. \tag{8}$$

The shape functions constructed by PIM have the Kronecker delta function property, which allows the simple imposition of essential boundary conditions as in conventional FEM.

The PIM is accurate and easy to use. However, an inappropriate choice of polynomial basis terms or the bad arrangement of nodes in the support domain near $\mathbf{X}$ will result in a singular matrix $\mathbf{P}_Q$. Several strategies have been proposed to overcome this problem [16]. Using radial basis functions (RBF) is one of the best solutions to guarantee the invertability of $\mathbf{P}_Q$. There are different functions such as multi-quadratic, Gaussian, and Logarithmic that can be used as RBF. In this paper the multi-quadratic form has been used as follows:

$$R_i(\mathbf{X}) = [r_i + c^2]^q, \tag{9}$$

where r_i is the distance between the desired point ($\mathbf{X}$) and field node $i(\mathbf{X}_i)$ defined as

$$r_i = [(x - x_i)^2 + (y - y_i)^2]^{0.5}, \tag{10}$$

c and q in Eq. (9) are constants having best values that should be determined during solution, and depend on the type of problem. For the solid mechanic problems, Liu [15] suggests 1.42 and 0.98 for c and q, respectively. The mentioned values are used in this paper.

To ensure the consistency of RPIM, polynomial terms are added to pure radial basis functions. This also improves the accuracy of the results. So the approximation of function $u(\mathbf{X})$ can be written as

$$u(\mathbf{X}) = \sum_{i}^{n} R_i(\mathbf{X})a_i + \sum_{j}^{m} p_j(\mathbf{X})b_j = \mathbf{R}^T(\mathbf{X})\mathbf{a} + \mathbf{P}^T(\mathbf{X})\mathbf{b}, \tag{11}$$

where

$$\mathbf{R}(\mathbf{X}) = [R_1(\mathbf{X}) \quad R_2(\mathbf{X}) \quad R_3(\mathbf{X}) \quad \dots \quad R_n(\mathbf{X})]^T, \tag{12}$$

$$\mathbf{P}(\mathbf{X}) = [p_1(\mathbf{X}) \quad p_2(\mathbf{X}) \quad p_3(\mathbf{X}) \quad \cdots \quad p_n(\mathbf{X})]^T, \tag{13}$$

$$\mathbf{a} = [a_1 \quad a_2 \quad a_3 \quad \dots \quad a_n]^T, \tag{14}$$

$$\mathbf{b} = [b_1 \quad b_2 \quad b_3 \quad \dots \quad b_m]^T, \tag{15}$$

where R_i and p_j are the radial and polynomial basis function respectively, a_i and b_j are interpolation coefficients, m is the number of polynomial terms and n is the number of nodes in the support domain of $\mathbf{X}$. For a_i and b_j determination, $m + n$ equations are needed. n equation can be produced by enforcing $u(\mathbf{X})$ to be the nodal displacement at n nodes in the support domain. So we have

$$u_k = u(x_k, y_k) = \sum_{i=1}^{n} R_i(x_k, y_k)a_i + \sum_{j=1}^{m} p_j(x_k, y_k)b_j, \quad k = 1, 2, \dots, n \tag{16}$$

or in matrix form

$$\mathbf{U}_S = \mathbf{R}_Q\mathbf{a} + \mathbf{P}_m\mathbf{b}, \tag{17}$$

where

$$\mathbf{R}_Q = \begin{bmatrix} R_1(r_1) & R_2(r_1) & \cdots & R_n(r_1) \\ R_1(r_2) & R_2(r_2) & \cdots & R_n(r_2) \\ \vdots & \vdots & & \vdots \\ R_1(r_n) & R_2(r_n) & \cdots & R_n(r_n) \end{bmatrix}_{n\times n}, \tag{18}$$

$$\mathbf{P}_m = \begin{bmatrix} p_1(x_1, y_1) & p_2(x_1, y_1) & \cdots & p_m(x_1, y_1) \\ p_1(x_2, y_2) & p_2(x_2, y_2) & \cdots & p_m(x_2, y_2) \\ \vdots & \vdots & & \vdots \\ p_1(x_n, y_n) & p_2(x_n, y_n) & \cdots & p_m(x_n, y_n) \end{bmatrix}_{n\times m}, \tag{19}$$

m remained equations can be gained through

$$\sum_{i=1}^{n} p_j(x_i, y_i)a_i = 0, \quad j = 1, 2, \ldots, m, \tag{20}$$

which is the uniqueness condition for solutions.

In matrix form Eq. (20) can be written as

$$\mathbf{P}_m^T \mathbf{a} = 0. \tag{21}$$

Combining Eqs. (17) and (21) gives

$$\overline{\mathbf{U}}_S = \begin{Bmatrix} \mathbf{U}_S \\ \mathbf{0} \end{Bmatrix} \underbrace{\begin{bmatrix} \mathbf{R}_Q & \mathbf{P}_m \\ \mathbf{P}_m^T & \mathbf{0} \end{bmatrix}}_{G} \begin{Bmatrix} \mathbf{a} \\ \mathbf{b} \end{Bmatrix} = \mathbf{G}\mathbf{a}_0, \tag{22}$$

where

$$\mathbf{a}_0 = \{ a_1 \quad a_2 \quad \cdots \quad a_n \quad b_1 \quad b_2 \quad \cdots \quad b_m \}, \tag{23}$$

$$\overline{\mathbf{U}}_S = \{ u_1 \quad u_2 \quad \cdots \quad u_n \quad 0 \quad 0 \quad \cdots \quad 0 \}. \tag{24}$$

From Eq. (22) we have

$$\mathbf{a}_0 = \begin{Bmatrix} \mathbf{a} \\ \mathbf{b} \end{Bmatrix} = \mathbf{G}^{-1}\overline{\mathbf{U}}_S. \tag{25}$$

A combination of Eqs. (11) and (25) gives

$$u(\mathbf{X}) = \{ \mathbf{R}^T(\mathbf{X}) \quad \mathbf{P}^T(\mathbf{X}) \}\mathbf{G}^{-1}\overline{\mathbf{U}}_\mathbf{S} = \overline{\mathbf{\Phi}}^\mathbf{T}(\mathbf{X})\overline{\mathbf{U}}_\mathbf{S}, \tag{26}$$

where

$$\overline{\mathbf{\Phi}}^T = \{ \varphi_1(\mathbf{X}) \quad \varphi_2(\mathbf{X}) \quad \cdots \quad \varphi_n(\mathbf{X}) \quad \varphi_{n+1}(\mathbf{X}) \quad \cdots \quad \varphi_{n+m}(X) \} \tag{27}$$

and the vector of shape functions is as follows:

$$\mathbf{\Phi}^T = \{ \varphi_1(\mathbf{X}) \quad \varphi_2(\mathbf{X}) \quad \cdots \quad \varphi_n(\mathbf{X}) \}. \tag{28}$$

3. Reinforced soil analysis

Two points of view are considered in the numerical analysis of reinforced structures. The first one is the composite representation in which the reinforced system is represented as an equivalent homogeneous anisotropic material; the composite properties reflect the properties of the constituent materials and their interaction. The second is the discrete representation in which each constituent material is investigated separately, so the reinforced soil system is divided into three separate parts. These parts include soil, reinforcements, and interface layers. In this paper discrete representation has been used to analyze the reinforced soil system. In the rest of this section, the general form of equations for the boundary value problems in plane strain conditions are expressed in each part of the reinforced soil system (i.e. soil, reinforcements and interface layers). Then the modified variational principles for discontinuous media are established, and finally, the discrete system of equations for reinforced soil analysis is derived.

4. General equations for plane strain problems

4.1. Static equilibrium equation

For a solid defied in domain Ω, the static equilibrium equation (strong form) can be given as

$$\mathbf{L}^T\boldsymbol{\sigma} + \mathbf{b} = 0, \tag{29}$$

where

$$\boldsymbol{\sigma}^T = \{ \sigma_x \quad \sigma_y \quad \sigma_z \quad \tau_{xy} \} \tag{30}$$

is the vector of stress and the operator $\mathbf{L}$ is as follows:

$$\mathbf{L}^T = \begin{bmatrix} \frac{\partial}{\partial x} & 0 & 0 & \frac{\partial}{\partial y} \\ 0 & \frac{\partial}{\partial y} & 0 & \frac{\partial}{\partial x} \\ 0 & 0 & \frac{\partial}{\partial z} & 0 \end{bmatrix} \tag{31}$$

and the body force density vector **b** is

$$\mathbf{b}^T = \{ b_x \quad b_y \quad b_z \} \tag{32}$$

It should be noted that the out of plane component of stress is considered due to plastic analysis.

5. Strain–displacement relation

5.1. Soil and reinforcements

Since there is no relation between the shape functions and mesh construction in MFM, unlike FEM, reinforcement can be modeled as two dimensional mediums. So at each arbitrary point in the soil or the reinforcement, the strain–displacement relation is as follows:

$$\boldsymbol{\varepsilon} = \boldsymbol{\Delta}^T \mathbf{u}, \tag{33}$$

where the strain tensor is

$$\boldsymbol{\varepsilon}^T = \{ \varepsilon_x \quad \varepsilon_y \quad \varepsilon_z \quad \gamma_{xy} \} \tag{34}$$

and

$$\boldsymbol{\Delta} = \begin{bmatrix} \frac{\partial}{\partial x} & 0 & 0 & \frac{\partial}{\partial y} \\ 0 & \frac{\partial}{\partial y} & 0 & \frac{\partial}{\partial x} \end{bmatrix} \tag{35}$$

and the vector of displacement is

$$\mathbf{u}^T = \{ u \quad v \}. \tag{36}$$

Using Eqs. (7) and (33) the strain–displacement relation in each support domain can be written as

$$\boldsymbol{\varepsilon} = \mathbf{B}\mathbf{U}_S, \tag{37}$$

where $\mathbf{U}_S$ is the vector of nodal displacements, and **B** is as follows:

$$\mathbf{B} = \begin{bmatrix} \widetilde{\mathbf{B}}_{i1} & \widetilde{\mathbf{B}}_{i2} & \cdots & \widetilde{\mathbf{B}}_{ik} & \cdot & \widetilde{\mathbf{B}}_{in} \end{bmatrix}, \tag{38}$$

where

$$\widetilde{\mathbf{B}}_{ik} = \begin{bmatrix} \frac{\partial \varphi_{ik}}{\partial x} & 0 & 0 & \frac{\partial \varphi_{ik}}{\partial y} \\ 0 & \frac{\partial \varphi_{ik}}{\partial y} & 0 & \frac{\partial \varphi_{ik}}{\partial x} \end{bmatrix}^T \tag{39}$$

and $\varphi_{ik} = \varphi_k(x_i)$ is the shape function of kth node at ith node in the support domain.

6. Interface layer

The interface layer is the contact plane between two bodies with different material properties representing a thin "smeared" zone. In this paper, the concept of a linkage element has been used for interface modeling, hence the interface layer is considered as two parallel planes with an insignificant distance from each other. A series of springs are assumed between the planes. The springs are resistant to the relative normal and tangential displacement of planes. The stiffness of springs into the unit area (stiffness coefficient) along normal and tangential directions are k_n and k_s respectively. As shown in Fig. 2, point P is considered between the planes of the interface layer to determine the strain–displacement relationship. The width of interface (h) is much less than its length (L), hence the strain in the n direction in the interface can be assumed

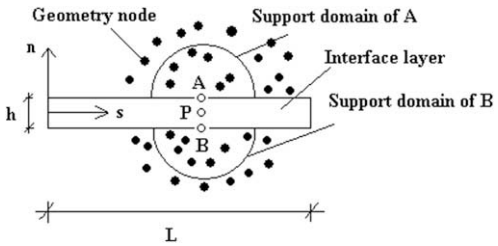

Fig. 2. Interface modeling.

to be constant. The relative displacement of point P can be related to the displacements of points A and B on the top and bottom planes as follows:

$$\boldsymbol{\delta} = [\,\delta_s \quad \delta_n\,]^T = \overline{\mathbf{U}}_B - \overline{\mathbf{U}}_A, \tag{40}$$

where δ_n and δ_s are the normal and shear relative displacement of point P respectively, and $\overline{\mathbf{U}}_A$ and $\overline{\mathbf{U}}_B$ are displacement vectors of points A and B in local coordinate n–s respectively. Using the coordinate transform matrix ($\mathbf{C}$) the displacement vectors can be written as

$$\mathbf{U} = \mathbf{C}\overline{\mathbf{U}}. \tag{41}$$

On the other hand, the displacements of points A and B can be related to the displacements of the nodes in the support domain of those points (Fig. 2). So we have

$$\begin{aligned} \overline{\mathbf{U}}_A &= \boldsymbol{\Phi}_A \overline{\mathbf{u}}_{gA}, \\ \overline{\mathbf{U}}_B &= \boldsymbol{\Phi}_B \overline{\mathbf{u}}_{gB}, \end{aligned} \tag{42}$$

where $\boldsymbol{\Phi}_A$ and $\boldsymbol{\Phi}_B$ are the shape function matrices of the nodes in the support domains of point A and B respectively, and $\overline{\mathbf{u}}_{gA}$ and $\overline{\mathbf{u}}_{gB}$ are the displacement vectors of the nodes in the support domain of A and B respectively.

Considering Eqs. (40)–(42) we have

$$\boldsymbol{\delta} = \mathbf{B}_i \mathbf{U}_i, \tag{43}$$

where

$$\mathbf{B}_i = [-\mathbf{C}\boldsymbol{\Phi}_A \quad \mathbf{C}\boldsymbol{\Phi}_B\,], \tag{44}$$

$$\mathbf{U}_i^T = [\,\overline{\mathbf{u}}_{gA}^T \quad \overline{\mathbf{u}}_{gB}^T\,]. \tag{45}$$

.

Defining the strain tensor in the interface layer as

$$\boldsymbol{\varepsilon}_i = \{\,\gamma_{ns} \quad \varepsilon_n\,\}, \tag{46}$$

where γ_{ns} and ε_n are the shear and normal strain respectively, we can have

$$\boldsymbol{\varepsilon}_i = \frac{1}{h}\boldsymbol{\delta} \tag{47}$$

and by combination of Eqs. (43) and (47) the strain–displacement relation in the interface layer can be written as follows:

$$\varepsilon_i = \frac{1}{h}\mathbf{B}_i \mathbf{U}_i. \tag{48}$$

7. Stress–strain relationship

7.1. Soil and reinforcements

The stress–strain relationship in elastic analysis can be written as

$$\boldsymbol{\sigma} = \mathbf{D}_e \boldsymbol{\varepsilon}, \tag{49}$$

where according to the definition of stress and strain tensors we have

$$\mathbf{D}_e = \frac{E(1-\upsilon)}{(1+\upsilon)(1-2\upsilon)} \begin{bmatrix} 1 & \frac{\upsilon}{1-\upsilon} & \frac{\upsilon}{1-\upsilon} & 0 \\ \frac{\upsilon}{1-\upsilon} & 1 & \frac{\upsilon}{1-\upsilon} & 0 \\ \frac{\upsilon}{1-\upsilon} & \frac{\upsilon}{1-\upsilon} & 1 & 0 \\ 0 & 0 & 0 & \frac{1-2\upsilon}{2(1-\upsilon)} \end{bmatrix}, \tag{50}$$

where E and υ are the elastic modulus and the Poisson ratio of materials respectively.

In elasto-plastic analysis the stress–strain relation is as follows:

$$d\boldsymbol{\sigma} = \mathbf{D}_{ep} d\boldsymbol{\varepsilon}, \tag{51}$$

where

$$\mathbf{D}_{ep} = \mathbf{D}_e - \frac{\mathbf{D}_e \left\{\frac{\partial P}{\partial \sigma}\right\} \left\{\frac{\partial F}{\partial \sigma}\right\}^T \mathbf{D}_e}{\left\{\frac{\partial F}{\partial \sigma}\right\}^T \mathbf{D}_e \left\{\frac{\partial P}{\partial \sigma}\right\}}, \tag{52}$$

where F and P are yield and potential functions respectively.

In this paper the elastic–perfect plastic Mohr–Coulomb criterion has been used for soil behavior and the yield function is as follows:

$$F = \frac{1}{3} I_1 \sin\Theta + \sqrt{I_2}\left(\cos\theta - \frac{1}{\sqrt{3}}\sin\theta\sin\Theta\right) - \xi\cos\Theta, \tag{53}$$

where I_1 is the first invariant of stress, I_2 is the second invariant of deviatoric stress, Θ is an internal friction angle, θ is Lode angle and ξ is cohesion. If a non-associated flow rule is assumed, the dilation angle can be used instead of an internal friction angle for the potential function.

Eqs. (51) and (52) are also available for reinforcements and an arbitrary elasto-plastic model can be used.

8. Interface layer

Considering the strain tensor definition in the interface layer, the stress–strain relation in elastic analysis can be written as

$$\boldsymbol{\sigma}_i = \mathbf{D}_i(h\boldsymbol{\varepsilon}_i) = \mathbf{D}_i\boldsymbol{\delta}, \tag{54}$$

where

$$\boldsymbol{\sigma}_i = \{\tau \quad \sigma_n\}^T, \tag{55}$$

$$\mathbf{D}_i = \begin{bmatrix} k_s & 0 \\ 0 & k_n \end{bmatrix}, \tag{56}$$

where τ and σ_n are shear and normal stress in the interface layer respectively.

Considering the Mohr–Coulomb criterion, the yield and potential functions in elasto-plastic behavior can be written as

$$F = \tau - \sigma_n \tan\Theta, \tag{57}$$

$$P = \tau - \sigma_n \tan\psi. \tag{58}$$

Using Eqs. (51), (52), (57) and (58), the stress–strain relation can be derived as

$$\mathbf{d}\boldsymbol{\sigma}_i = \mathbf{D}_{epi}\mathbf{d}\boldsymbol{\varepsilon}_i, \tag{59}$$

$$\mathbf{D}_{epi} = \frac{1}{k_s + k_n \tan\Theta \tan\psi}\begin{bmatrix} k_s\, k_n \tan\Theta \tan\psi & k_s \tan\Theta\, \mathrm{sgn}(\tau) \\ k_n \tan\psi\, \mathrm{sgn}(\tau) & k_s\, k_n \end{bmatrix}, \tag{60}$$

where sgn is the sign function.

9. Variational principals for discontinuous mediums

Generally the total potential energy functional for a discontinuous media is expressed as

$$\Pi = \Pi_e + \Pi_i + \Pi_f, \tag{61}$$

where Π_e and Π_i are the elastic strain energy of a solid media and interface layer respectively, and Π_f is the potential energy related to external forces. These functionals can be defined as

$$\Pi_e = \int\int_\Omega \frac{1}{2}\boldsymbol{\varepsilon}^T\boldsymbol{\sigma}\, d\Omega, \tag{62}$$

$$\Pi_i = \int_\beta \frac{1}{2}\boldsymbol{\varepsilon}_i^T\boldsymbol{\sigma}_i\, d\beta, \tag{63}$$

$$\Pi_f = -\int_\Gamma \mathbf{U}^{\mathbf{T}}\overline{\mathbf{T}}\, d\Gamma - \int\int_\Omega \mathbf{U}^T\mathbf{b}\, d\Omega, \tag{64}$$

where β is the length parameter along the interface layer, $\overline{T}$ is the prescribed surface traction and Γ is the boundary along which the surface traction is imposed.

The variational (weak) form of Eq. (61) can be written as

$$\delta\Pi = \int\int_\Omega (\delta\boldsymbol{\varepsilon})^T\mathbf{D}\boldsymbol{\varepsilon}\, d\Omega + \int_\beta (\delta\boldsymbol{\varepsilon}_i)^T\mathbf{D}_i\boldsymbol{\varepsilon}\, d\beta - \int\int_\Omega (\delta\mathbf{U})^T\mathbf{b}\, d\Omega - \int_\Gamma (\delta\mathbf{U})^T\overline{\mathbf{T}}\, d\Gamma = 0. \tag{65}$$

Using the stress–strain relation, the discrete form of equations can be written as

$$\mathbf{KU} = \mathbf{F}, \tag{66}$$

$$\mathbf{K} = \int\int_{\Omega} \mathbf{B}^T \mathbf{D} \mathbf{B} d\Omega + \int_{\beta} \mathbf{B}_i^T \mathbf{D}_i \mathbf{B}_i d\beta, \tag{67}$$

$$\mathbf{F} = \int\int_{\Omega} \mathbf{\Phi}^T \mathbf{b} d\Omega + \int_{\Gamma} \mathbf{\Phi}^T \overline{\mathbf{T}} d\Gamma, \tag{68}$$

where

$$\mathbf{\Phi} = \left[\tilde{\mathbf{\Phi}}_{i1} \quad \tilde{\mathbf{\Phi}}_{i2} \quad \cdots \quad \tilde{\mathbf{\Phi}}_{ik} \quad \cdots \quad \tilde{\mathbf{\Phi}}_{in} \right], \tag{69}$$

$$\tilde{\mathbf{\Phi}}_{ik} = \begin{bmatrix} \varphi_{ik} & 0 \\ 0 & \varphi_{ik} \\ 0 & 0 \end{bmatrix}. \tag{70}$$

10. Problem solution

Using the MFM, the soil medium is represented by regular or irregular arrangement of nodes among which each reinforcement is represented by nodes arranged along two parallel lines. The distance between lines is equal to the thickness of the reinforcement. Soil and reinforcements are completely separate from each other, and the interface layers relate them in order to guarantee the compatibility of the whole problem.

After the geometry representation, a background mesh is used for each constituent of reinforced soil (i.e. soil, reinforcements and interface layers) for the numerical calculation of the integrals in Eqs. (67) and (68). In this paper the gauss integration rule has been used. After defining Gauss points (or quadrature points), a support domain is considered around each of them. In this paper circular domains are considered. The radiuses of support domains are different in different problems and depend on the distance of the nodes from each other. Usually it is desired that each support domain contains 5–30 nodes. As the reinforced soil is a discontinuous media, the visibility criterion is used for support domain definition. The visibility criterion defines the support domain of a node as the field of vision at the node. All boundaries, internal and external, are considered to be opaque so that the field of vision is interrupted when a boundary is encountered. Hence as shown in Fig. 3, node 1 is considered a node in the support domain of point X, but node 2 is not considered.

Supports of different parts are completely separate from each other, in other words, supports of quadrature points in soil media do not include the nodes of reinforcement and vice versa (Fig. 4). The compatibility condition is satisfied by the interface layer.

After defining support domains, the shape functions are constructed by the RPIM and the required matrices are formed according to Eqs. (67) and (68) and the general equation (66) is gained. Solving this equation determines unknown displacements, and consequently, stresses and strains at any point. Up to this stage, the elastic analysis is performed. For elasto-plastic analysis the modified Newton–Raphson method is used, hence only the elastic stiffness matrix is used. There is a stepwise imposition of external loads and in each step the unbalanced forces are calculated by the subtraction of nodal forces due to internal stresses from the nodal forces due to external stresses. By the minimization of the unbalanced forces in each step, the process of calculations goes ahead. The following criterion is used for passing each step to another

$$\frac{\|f_{\text{unb}}\|}{\|f_{\text{ext}}\|} < 0.001, \tag{71}$$

where $\|\cdot\|$ is Euclidean norm, f_{unb} is unbalanced nodal force and f_{ext} is external nodal force.

There are some cases in reinforced structure analyses such as the pull out test or slope stability, in which slippage or separation may occur between the reinforcement and the surrounding soil. Therefore the concept of the Herrmann [17] linkage

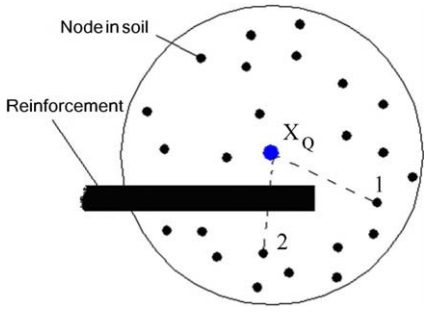

Fig. 3. Visibility criterion.

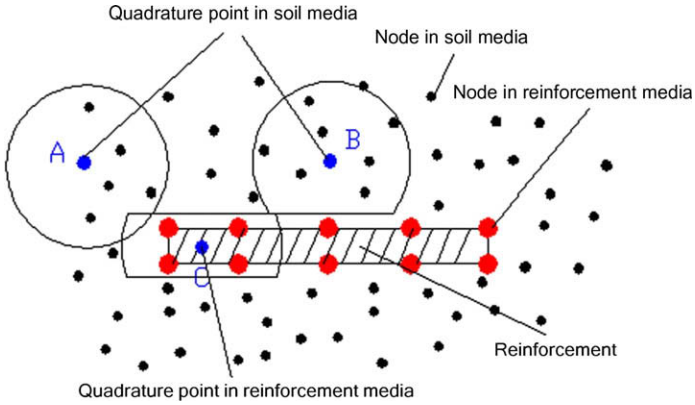

Fig. 4. Support domains in soil and reinforcement mediums.

element is adopted here to simulate these phenomena. According to Herrmann's approach, three distinct response regimes are defined as the non-slip, the slip and the separation modes. For an interface with no tensile strength, separation will occur when the normal relative displacement exceeds zero. Since forces cannot be transmitted across and along an open interface, the stiffness coefficients (k_s and k_n) are both zero. When there is no positive normal relative displacement, the shear stress should be investigated. If the shear stress (τ) reaches the shear strength of the interface (τ_{max}) (which is governed by the failure criterion) slippage takes place and the tangential stiffness coefficient (k_s) is set equal to zero. After slip, the interface can only support a shear stress equal to τ_{max}. The difference between τ and τ_{max} must be corrected and re-distributed to neighboring nodes. When none of the mentioned conditions occurs, a non-slip mode results.

11. Numerical study

In this section the developed code should be verified by solving some examples. Since the authors did not encounter any exact solution (without any simplification) for discontinuous media, the results of the developed code are verified by FEM codes. It is assumed that by increasing the number of elements the results of the FEM code gets closer to the exact solution.

11.1. Example (1). Elastic discontinuous media under concentrated load

In this example a reinforced media is considered in which the reinforcement is placed at the mid height of the column. A 50 KN concentrated load is imposed on top of the column. The geometry of the problem and the boundary conditions are shown in Fig. 5. The media is weightless and completely elastic with the elastic modulus and Poisson ratio equal to 3×10^4 KN/m^2 and 0.3 respectively. The reinforcement is also elastic and its elastic modulus and Poisson ratio are equal

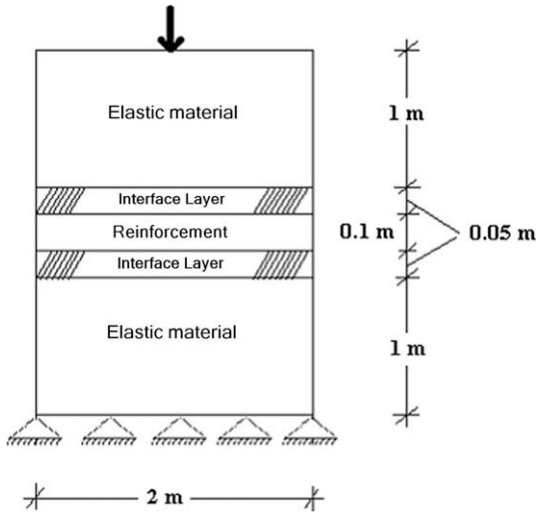

Fig. 5. Elastic reinforced column under concentrated load.

to 6×10^5 KN/m^2 and 0.25 respectively. Interface layers are considered on the top and bottom of the reinforcement. The normal and shear stiffness of the reinforcement are 10^4 KN/m^3 and 10^6 KN/m^3 respectively.

Since there is no exact solution for this problem, the FEM is used. By increasing the number of elements, a parameter is calculated as

$$\eta = \left| \frac{\|\mathbf{U}^P_{\text{FEM}}\| - \|\mathbf{U}^F_{\text{FEM}}\|}{\|\mathbf{U}^F_{\text{FEM}}\|} \right|, \tag{72}$$

where $\mathbf{U}^P_{\text{FEM}}$ and $\mathbf{U}^F_{\text{FEM}}$ are the vectors of displacement for the analysis with P number of elements and the analysis with the initial number of elements respectively. At any stage of analysis that, by increasing the number of elements the value of η remains constant, the results of the analysis can be assumed as a substitution for the exact solution.

In this example SIGMAW has been used as the FEM code. The reason for the selection of this software is that it has slip elements and the interface layer can be modeled easily, also the finite element modeling is the most similar to mesh-free simulation. However, the mentioned conditions only exist for elastic analysis. The initial solution started with four elements for the elastic medium, two elements for reinforcement and two elements for interface layers (Fig. 6). By increasing the number of elements and a comparison of the results with the initial solution, η is calculated at every stage of the analysis. Fig. 7 shows the variation of η with respect to the number of elements. According to this figure, the finite element model, with 992 elements (896 elements for elastic medium and 32 elements for reinforcement and each interface layer) can be substituted for the exact solution.

Now the convergence of MFM should be investigated for this problem. As shown in Fig. 8, three mesh-free models are assumed. In the first model the distance between nodes is 1 m and the geometry of the problem is defined by 12 nodes for the elastic medium and six nodes for reinforcement (in total 18 nodes). In the second and third model the distance between nodes decreased to 0.5 m and 0.25 m respectively, in which 40 and 100 nodes were produced respectively. In all models a 4×4 background mesh with 16 quadrature points in each block (Fig. 9) is considered for integration. The radiuses of support domains were different in different models. Hence in the model with 18 nodes the 1.5 m radius has been used, and in models with 40 and 100 nodes the 1 m and 0.7 m radiuses have been used respectively. The relative error of displacement between the MFM and the FEM (which is the substitution for exact solution) can be determined as follows:

$$e_d = \frac{\sum_{i=1}^{N} |u_i^{\text{MFM}} - u_i^{\text{FEM}}|}{\sum_{i=1}^{N} |u_i^{\text{FEM}}|}, \tag{73}$$

where e_d is the relative error of displacement, u_i^{MFM} is the displacement of node i in MFM, u_i^{FEM} is the displacement of node i in FEM and N is the number of considered nodes. Fig. 10 shows the variation of e_d with respect to the distances between nodes in a logarithmic scale. It is obvious that by decreasing the distances between nodes, the relative error is also decreased. This condition confirms the convergence of the method. In Table 1 the results of MFM and FEM for the displacement of the 90 node mesh-free model (Fig. 8c) has been shown. The results are presented for the nodes numbers shown in Fig. 8a. Due to the symmetry of the model, the results for a half model are shown. In the last column of Table 1 the total errors of displacements between MFM and FEM are represented. As shown, the results have very good agreement with each other and the maximum error is less than 11%. The result of this example shows the good performance of MFM in elastic discontinuous media.

11.2. Example (2). Pull-out test

In this example a two dimensional pull-out test is simulated. This problem has been investigated by Coutinho et al. [18] to verify their new zero thickness kinematically consistent interface element. As shown in Fig. 11, in the finite element model the continuum is simulated by 48 quadrilateral elements, the bar by 12 truss elements and the interface layer by 12 zero thickness elements at each side of the bar. The upper interface elements are numbered from 1 to 12.

The plastic behavior of the interface is governed by Mohr–Coulomb criterion with a null cohesion and a friction coefficient equal to 0.5. The normal and tangential stiffness coefficients of the interface are 10^{10} KN/m^3 and 10^6 KN/m^3 respectively. The continuum is elastic with $E = 2000$ KN/m^2 and $\nu = 0.25$ and a plane strain state is assumed. The one-dimensional bar

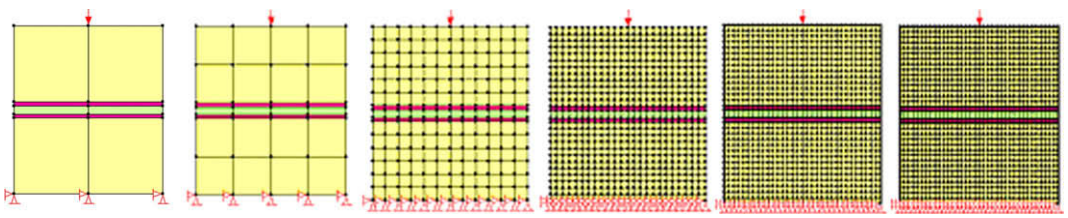

Fig. 6. Finite element models by increasing the number of elements from left to right.

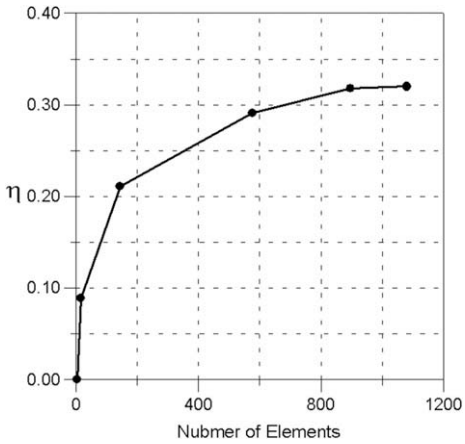

Fig. 7. Variation of η with respect to the number of elements.

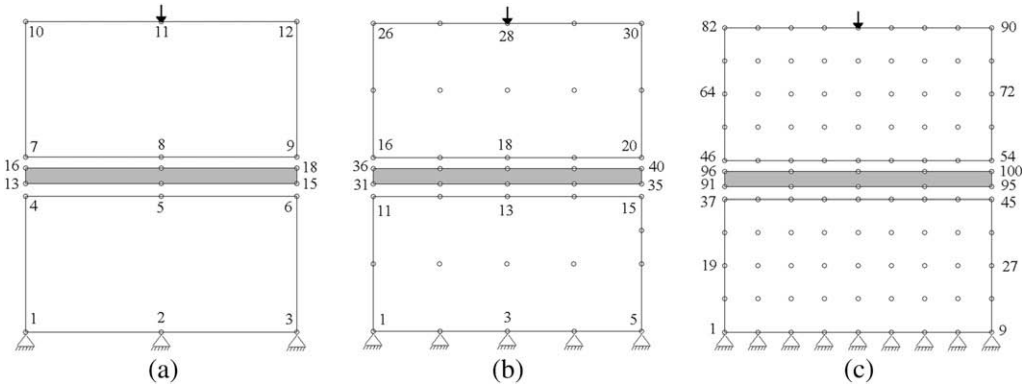

Fig. 8. Mesh-free models.

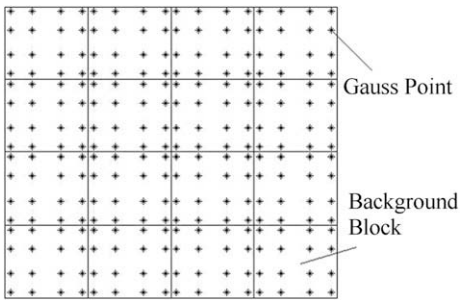

Fig. 9. Background mesh.

is also elastic with $E = 20,000\ \mathrm{KN/m^2}$ and a cross section area of 0.1 $\mathrm{m^2}$. The normal compression load is maintained constant and the horizontal force F_h is monotonically increased form zero to 60 kN.

This test is also simulated by the mesh-free method. As shown in Fig. 12 the continuum is modeled by 78 nodes and the bar by 26 nodes arranged along two parallel lines separated from each other by the thickness of the bar (i.e. 0.1). As the results of Coutinho's analysis are represented for the average values at the center of each element, the interface layers in each side of the bar in MFM are divided into 12 sub-interfaces with a thickness of 0.005 m and the results are shown for the average in each sub-interface. A 10×6 background mesh with four quadrature points in each block has been used for integration. The same properties of FEM have been used for the mesh-free model.

The distributions of normal and shear stresses along the upper interface in the finite element and mesh-free model for different F_h are presented in Figs. 13–16. These stresses are at the center of each sub-interface. As shown in Figs. 13–16 there

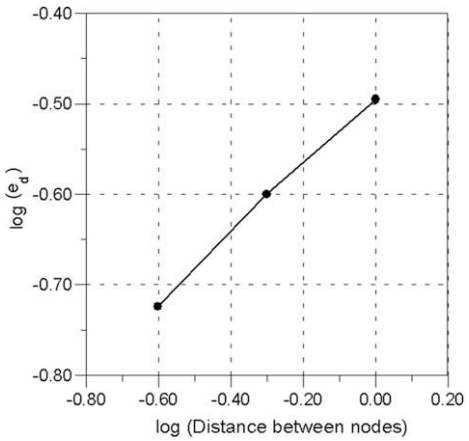

Fig. 10. Convergence investigation.

Table 1
The results of finite element model with 992 elements and mesh-free model with 90 nodes.

Node no.	FEM		MFM		Total error
	X-displacement	*Y*-displacement	*X*-displacement	*Y*-displacement	%
4	−1.71E−04	−4.91E−04	−1.35E−04	−4.78E−04	7.482081
5	0	−8.86E−04	0	−8.18E−04	7.726165
7	−4.89E−04	−5.26E−04	−4.26E−04	−5.65E−04	10.35843
8	0	−9.67E−04	0	−8.96E−04	7.335788
10	1.95E−04	−5.46E−04	1.84E−04	−5.34E−04	2.804887
11	0	−5.11E−03	0	−4.55E−03	10.9589
13	−6.69E−05	−5.06E−04	−6.58E−05	−5.13E−04	1.468459
14	0	−9.22E−04	0	−8.54E−04	7.374702
16	−3.02E−05	−5.08E−04	−1.97E−05	−5.16E−04	2.542262
17	0	−9.29E−04	0	−8.61E−04	7.345441

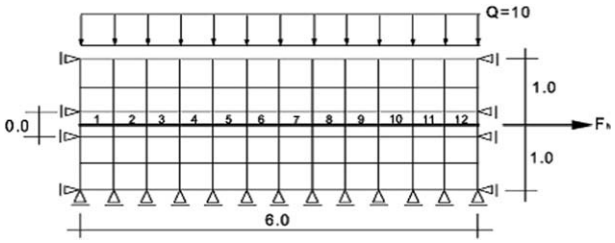

Fig. 11. Pull-out test modeling [17].

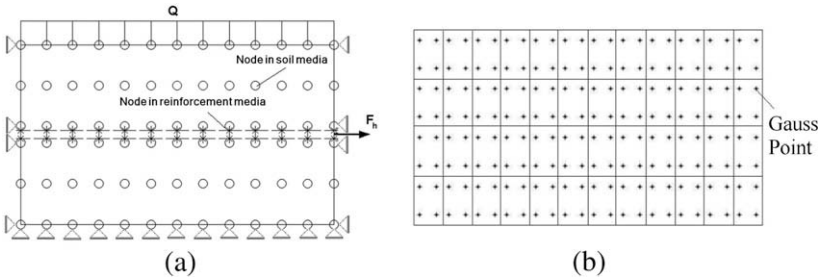

Fig. 12. (a) Mesh-free model; (b) background mesh.

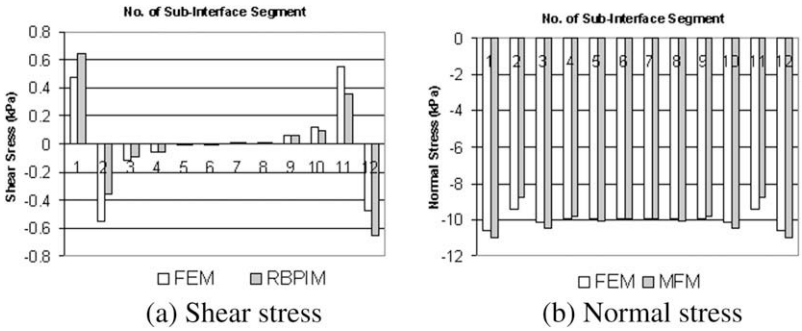

Fig. 13. Stress distribution for $F_h = 0$.

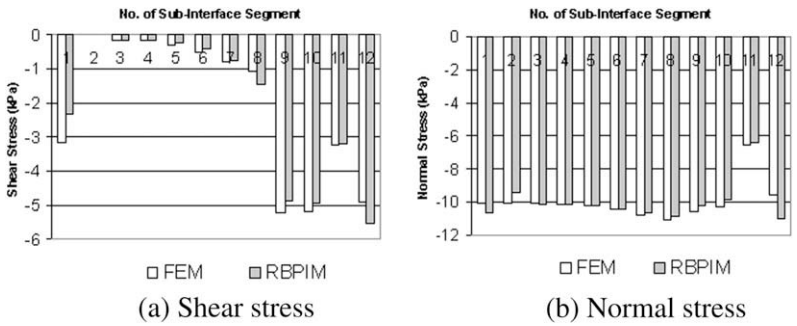

Fig. 14. Stress distribution for $F_h = 25$ KN.

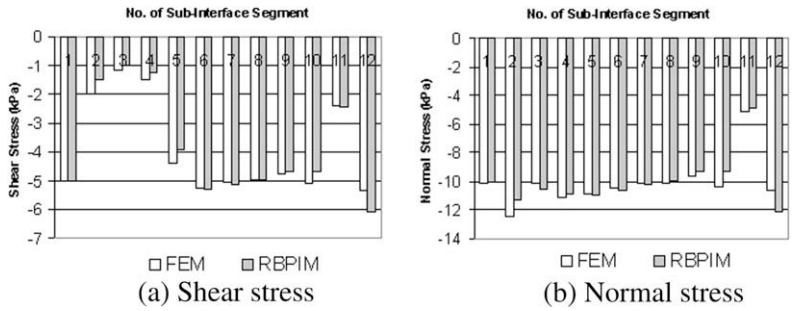

Fig. 15. Stress distribution for $F_h = 50$ KN.

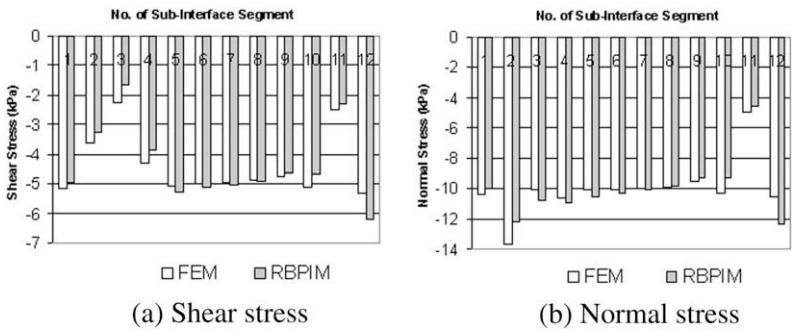

Fig. 16. Stress distribution for $F_h = 57.5$ KN.

is very good agreement between the stress distributions in FEM and MFM. This is especially obvious for the pattern of distribution. These results confirm the acceptability of interface modeling and the capability of the developed code for slippage simulation.

11.3. Example (3). Flexible footing on reinforced soil

A flexible strip footing with a 2 m width, exerted uniform load on a 10 m × 6 m reinforced soil box. According to Fig. 17 three patterns of reinforcement arrangement are considered. It is desired to determine the load–deformation curve at the mid point beneath the foundation for FEM (that by increasing the number of elements can be substituted by exact solution) and MFM and compare the results. The geometry of the problem and the pattern of reinforcement arrangement are shown in Fig. 17. The soil is assumed weightless and an elasto-plastic material with obedience from Mohr–Coulomb criterion.

The properties of soil are as follows: elastic modulus: $30,000\ \mathrm{KN/m^2}$, Poisson ratio: 0.3, cohesion: 20 KPa, internal friction angle: 25° and a dilation angle of 5° for non-associated behavior.

Reinforcements are elastic material with an elastic modulus and a Poisson ratio of $600,000\ \mathrm{KN/m^2}$ and 0.3 respectively. The thickness of reinforcements and interface layers are considered 0.01 m and 0.005 m respectively.

For finite element modeling PLAXIS, which is a robust finite element program for soil and rock analysis, has been used. This software generates mesh automatically and the user can refine the mesh at any stage with respect to the previous one. Hence the finest mesh that the software is able to generate is considered as a substitution for the exact solution. So for the patterns with a 1, 2 and 3 number of reinforcements, models with 2312, 2248 and 2182 number of elements have been used. In PLAXIS reinforcements are considered one-dimensional elements with only the axial stiffness. There is also an interface modeling with a strength reduction factor ($R_{\mathrm{inter}} \leqslant 1$). Considering the Mohr–Coulomb failure criterion, the following relations exist between the shear strength parameters of soil and interface

$$\xi_i = R_{\mathrm{inter}}\xi_{\mathrm{soil}}, \tag{74}$$

$$\tan(\Theta_i) = R_{\mathrm{inter}}\tan(\Theta_{\mathrm{soil}}) \leqslant \tan(\Theta_{\mathrm{soil}}), \tag{75}$$

where ξ_i and ξ_{soil} are the cohesion of the interface and soil respectively, and Θ_i and Θ_{soil} are the internal friction angle of the interface and soil respectively. The analyses in FEM have been performed for two different values of R_{inter}.

As shown in Fig. 18a, in the MFM 360 nodes with a regular arrangement are used for soil representation. Each reinforcement is modeled by 26 nodes along two parallel lines (which are separate from each other by the thickness of reinforcement). A 15 × 10 background mesh with four quadrature points in each block is used for integration (Fig. 18b). The radius of the support domain is considered 1 m. To be compatible with PLAXIS analyses the stiffness coefficients have been determined by the following equation:

$$D_i = \begin{bmatrix} k_s & 0 \\ 0 & k_n \end{bmatrix} = \begin{bmatrix} \frac{G_i}{t_i} & 0 \\ 0 & \frac{E_{ode,i}}{t_i} \end{bmatrix}, \tag{76}$$

where

$$E_{\mathrm{ode},i} = 2G_i\frac{1-\upsilon_i}{1-2\upsilon_i}, \quad G_i = R_{\mathrm{inter}}^2 G_{\mathrm{soil}} \leqslant G_{\mathrm{soil}}, \quad \upsilon_i = 0.45. \tag{77}$$

In Fig. 19 the load–deformation curves for three patterns of reinforcement arrangement are represented for the MFM and the FEM (i.e. PLAXIS). The complete bonding between soil and reinforcements is assumed in these curves ($R_{\mathrm{inter}} = 1$). In Fig. 20 similar curves to Fig. 19 are represented for $R_{\mathrm{inter}} = 0.7$. It is obvious from these figures that there is very good agreement between the results of the MFM and the FEM, which is substituted for the exact solution. So it can confirm the good performance of the developed code in the general case of elasto-plastic behavior of soil.

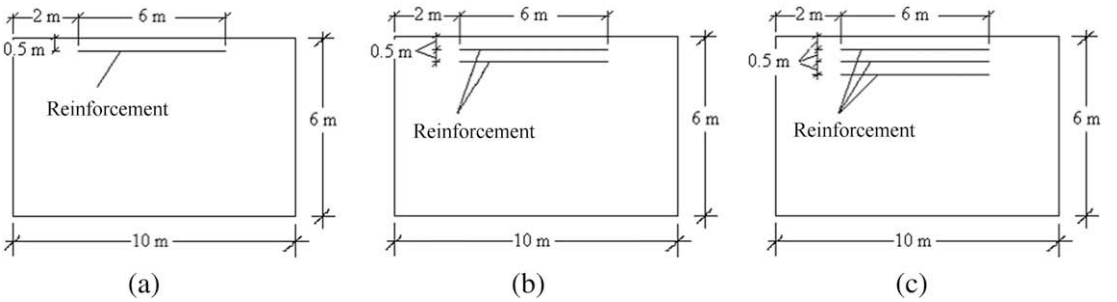

Fig. 17. Patterns of reinforcement arrangement.

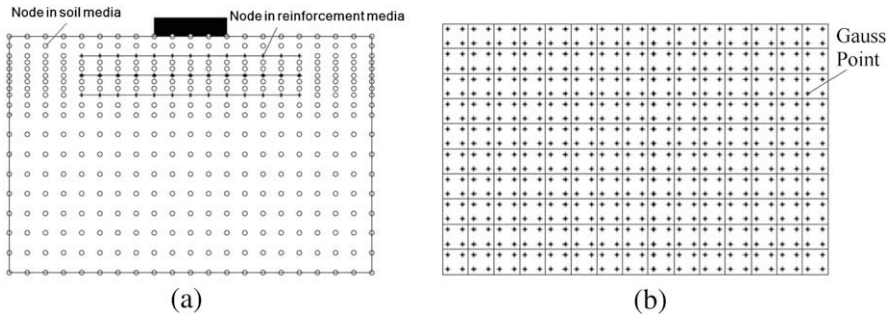

Fig. 18. (a) Mesh-free model (b) background mesh.

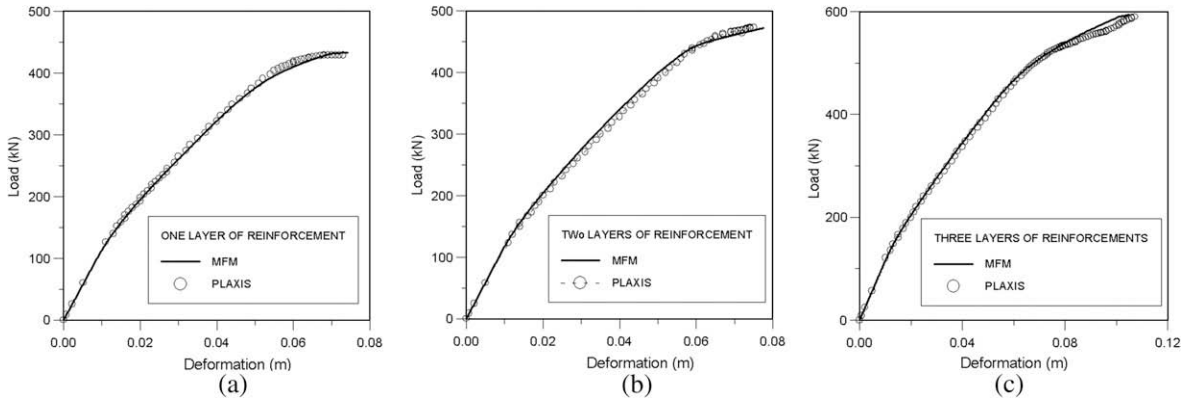

Fig. 19. Load–deformation curve at mid point beneath the foundation for the model with (a) one (b) two (c)three reinforcement layers for $R_{\text{inrt}} = 1$.

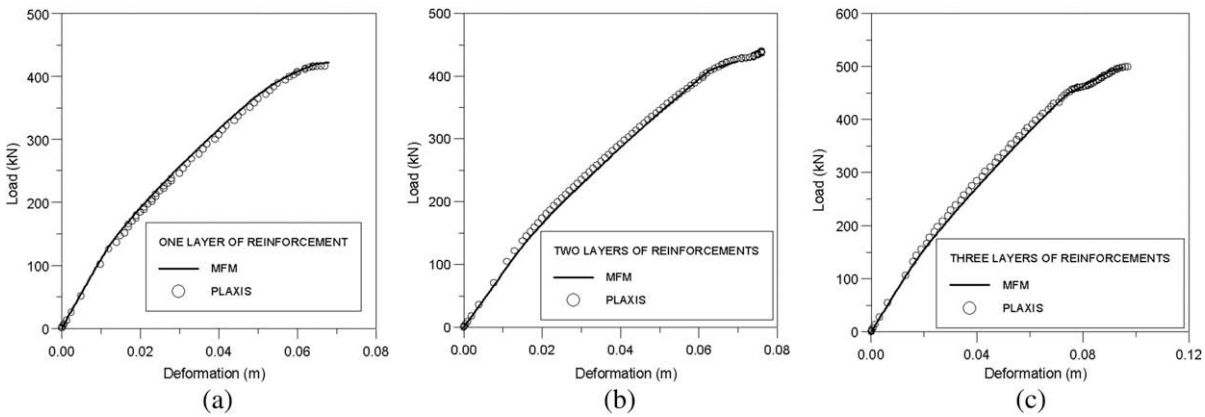

Fig. 20. Load–deformation curve at mid point beneath the foundation for the model with (a) one (b) two (c) three reinforcement layers for $R_{\text{inrt}} = 0.75$.

12. Conclusion

In this paper the application of the radial basis point interpolation method as an MFM for the elasto-plastic analysis of reinforced soils is studied for the first time. There is no need of mesh in the traditional sense and the shape functions are based on nodes. A background mesh is used just for numerical integration. The results of the analyses with the MFM and the FEM (which is substituted for exact solution) show very good agreement with each other. Hence in examples 1 and 3 the results of the MFM with quite a low number of nodes have very good agreement with the results of the FEM with a high number of elements. This can be a positive outlook for the application of mesh-free methods in reinforced soils analysis. However, as the present study is the first one in this category, it is too soon to conclude generally, and more theoretical and experimental research is needed.

References

[1] L.B. Lucy, A numerical approach to the testing of fission hypothesis, The Astronomical Journal 82 (12) (1977) 1013–1024.
[2] L.D. Libersky, A.G. Petschek, Smoothed particle hydrodynamics with strength of materials, Proceedings of the Next Free Lagrange Conference (1991) 248–257.
[3] B. Nayroles, G. Touzot, p. Villon, Generalizing the finite element method: diffuse approximation and diffuse elements, Computational Mechanics 10 (1992) 307–318.
[4] T. Belytschko, Y.Y. Lu, L. Gu, Element-free Galerkin methods, International Journal for Numerical Methods in Engineering 37 (1994) 229–256.
[5] C. Duarte, J.T. Oden, An hp adaptive method using clouds, Computer Methods in Applied Mechanics and Engineering 139 (1996) 237–262.
[6] W.K. Liu, S. Jun, Y.F. Zhang, Reproducing kernel particle methods, International Journal for Numerical Methods in Engineering 20 (1995) 1081–1106.
[7] G.R. Liu, Y.T. Gu, A point interpolation method for two-dimensional solids, International Journal for Numerical Methods in Engineering 50 (2001) 937–951.
[8] X. Zhang, M. Lu, J.L. Wegner, A 2-D meshless model for jointed rock structures, International Journal for Numerical Methods in Engineering 47 (2000) 1649–1661.
[9] N. Hataf, M. Hajazizi, A. Ghahramani, Mechanical analysis of jointed rock mass using meshless method and by imposition of penalty method, Sharif Journal 34 (40) (2007).
[10] J.G. Wang, G.R. Liu, Y.G. Wu, A point interpolation method for simulating dissipation process of consolidation, Computer Methods in Applied Mechanics and Engineering 190 (2001) 5907–5922.
[11] W.D. Wang, J.G. Wang, Z.L. Wang, T. Nogami, An unequal-order radial interpolation meshless method for Biot's consolidation theory, Computers and Geotechnics 34 (2007) 61–70.
[12] L. Guangxin, G. Jinhong, J. Yuxin, Free surface seepage analysis based on the element-free method, Mechanics Research Communications 30 (2003) 9–19.
[13] Z. Wiezckowski, The material point method in large strain engineering problems, Computer Methods in Applied Mechanics and Engineering 193 (2004) 4417–4438.
[14] S.M. Binesh, N. Hataf, A. Ghahramani, Elastic analysis of reinforced soil using point interpolation method, Journal of Iranian Science and Technology 31 (B5) (2007) 577–581.
[15] S.M. Binesh, N. Hataf, A. Ghahramani, Elastic analysis of discontinuous medium using mesh-free method, Journal of Applied Sciences 8 (19) (2008) 3389–3397.
[16] G.R. Liu, Mesh Free Methods: Moving Beyond the Finite Element Method, CRC Press, Florida, 2002. p. 171.
[17] L.R. Herrmann, Finite element analysis of contact problems, ASCE, Journal of Engineering Mechanics Division 104 (5) (1978) 1043–1057.
[18] A. Coutinho, M. Martin, R. Sydenstricker, J. Alves, L. Landau, Simple zero thickness kinematically consistent interface elements, Computers and Geotechnics 30 (2003) 347–374.